Inorg. Chem. **2006**, *45*, 4396–4406

Metal–Metal Bonding in Mixed Valence Ni_2^{5+} Complexes and Spectroscopic Evidence for a Ni_2^{6+} Species

John F. Berry,[†,‡] Eberhard Bothe,[‡] F. Albert Cotton,*[,†] Sergey A. Ibragimov,[†] Carlos A. Murillo,*[,†] Dino Villagrán,[†] and Xiaoping Wang[†]

Department of Chemistry and Laboratory for Molecular Structure and Bonding, P.O. Box 30012, Texas A&M University, College Station, Texas 77842-3012, and the Max-Planck-Institut für Bioanorganische Chemie, Stiftstrasse 34-36, D-45470 Mülheim an der Ruhr, Germany

Received January 20, 2006

Dinickel(II) complexes of the ligands *N,N′*-di-*p*-anisylformamidinate (DAniF) and *N,N′,N″*-triphenylguanidinate (TPG) have been synthesized and crystallographically characterized, along with their one-electron-oxidized analogues. In both systems, the Ni–Ni distances become shorter by ∼0.1 Å upon oxidation, in accord with the proposal that the resulting Ni_2^{5+} complexes are appropriately described as having one electron removed from a metal-based σ^* orbital and an overall Ni–Ni bond order of 1/2. Although conventional DFT calculations on the model compounds $Ni_2(HNCHNH)_4$ and $[Ni_2(HNCHNH)_4]^+$ appear to predict that the lowest energy state of the latter species would have one unpaired electron in an essentially ligand-based orbital. A single-point calculation of $Ni_2(DAniF)_4$ employing the geometry of its crystal structure with the full ligand included reveals a reversal of the previously predicted order of the HOMO and HOMO-1, and suggests that the unpaired electron in $[Ni_2(DAniF)_4]^+$ is in a metal-based orbital of σ^* symmetry. This is verified by the axial EPR spectrum of the compound in solution. The compound $Ni_2(DAniF)_4$ shows an unexpectedly rich cyclic voltammogram with four stepwise reversible oxidation waves. Coulometric experiments show that the doubly oxidized species has a significant lifetime at –25 °C, and by spectroelectrochemistry, its UV–vis spectrum was recorded. We propose that this species contains a Ni_2^{6+} core with a single Ni–Ni σ bond.

Introduction

Bond formation between transition metal atoms is the main direction of the studies in our research group.[1] Since the description of the quadruple bond in the $[Re_2Cl_8]^{2-}$ anion in 1963,[2] hundreds of compounds with different transition metals and different bond orders have been prepared and characterized,[3] many of which have important uses as catalysts,[4] in biological systems,[5] or as chemical sensors.[6] One transition element for which authentic examples of metal−metal bonding in lantern-type complexes remain scant is nickel,[7] although it should be mentioned that several low-valent organometallic complexes possessing Ni−Ni bonds have been described.[8]

Nickel-to-nickel bonds were first proposed in 1953 to explain the seemingly anomalous insolubility of nickel(II)-(bis-dimethylglyoxime) (**I**) as compared to its copper analogue.[9] Also, nickel−nickel bonding has been proposed in the dinuclear oxidation products of certain $Ni(L)_2$ complexes[10] (**II**) which also contain Ni^{II} (the oxidation having been shown to be ligand based[11]). In both of the above

* To whom correspondence should be addressed. E-mail: cotton@tamu.edu (F.A.C.); murillo@tamu.edu (C.A.M.).
† Texas A&M University.
‡ Max-Planck-Institut für Bioanorganische Chemie.

(1) Cotton, F. A. *Inorg. Chem.* **1998**, *37*, 5710.
(2) (a) Robinson, W. T.; Fergusson, J. E.; Penfold, B. R. *Proc. Chem. Soc. London* **1963**, 116. (b) Bertrand, J. A.; Dollase, W. A.; Cotton, F. A. *J. Am. Chem. Soc.* **1963**, *85*, 1349.
(3) Cotton, F. A.; Walton, R. A. *Multiple Bonds between Metal Atoms*, 2nd ed.; Clarendon Press: Oxford, 1993.
(4) See for example: Doyle, M. P.; Ren, T. *Prog. Inorg. Chem.* **2001**, *49*, 113.
(5) Chifotides, H. T.; Dunbar, K. R. *Acc. Chem. Res.* **2005**, *38*, 146.
(6) Hilderbrand, S. A.; Lim, M. H.; Lippard, S. J. *J. Am. Chem. Soc.* **2004**, *126*, 4972.
(7) Murillo, C. A. In *Multiple Bonds between Metal Atoms*, 3rd ed.; Cotton, F. A., Murillo, C. A., Walton, R. A., Eds.; Springer Science and Business Media, Inc.: New York, 2005.
(8) Denninger, U.; Schneider, J. J.; Wilke, G.; Goddard, R.; Kruger, C. *Inorg. Chim. Acta* **1993**, *213*, 129.
(9) (a) Godycki, L. E.; Rundle, R. E. *Acta Crystallogr.* **1953**, *6*, 487. (b) Banks, C. V.; Anderson, S. *J. Am. Chem. Soc.* **1962**, *84*, 1486.
(10) (a) Peng, S. M.; Ibers, J. A.; Millar, M.; Holm, R. H. *J. Am. Chem. Soc.* **1976**, *98*, 8037. (b) Peng, S. M.; Goedken, V. L. *J. Am. Chem. Soc.* **1976**, *98*, 8500.

10.1021/ic060125q CCC: $33.50
Published on Web 05/02/2006

situations, the Ni···Ni separations are quite long (≥3.0 Å) and no MO description of the supposed "bonding" between the two d^8 Ni^{II} ions has yet been given.[12] There is also a report of dinuclear nickel(II) monothiocarboxylates which suggests the possibility of Ni−Ni bonds on the basis of a magnetic study.[13] The dithioacetate complex $Ni_2(S_2CCH_3)_4$, which has a nickel−nickel separation (2.564(1) Å), has been oxidized by reaction with iodine.[14] The structure shows linear chains of ···I···$[Ni_2S_8]$···I···$[Ni_2S_8]$··· with a Ni−Ni distance of 2.514(3) Å. Because this compound is reported to be EPR silent, assignment of a metal−metal bond to this compound is ambiguous. It was not until our first investigation of Ni_2^{4+} and Ni_2^{5+} species (and their corresponding dipalladium analogues) with the lantern-type structure (**III**) that the

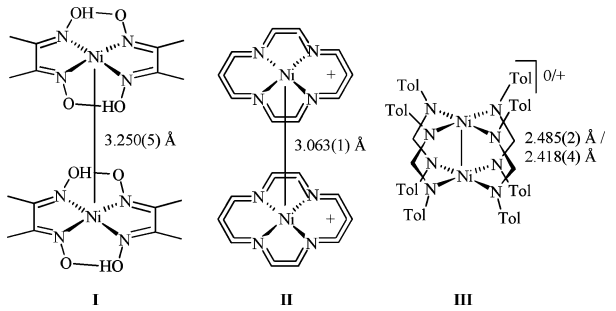

I **II** **III**

ground rules for Ni−Ni bond formation were laid out and demonstrated experimentally and theoretically.[15] Until our present work, this was the only unambiguous report of a lantern-type compound with a Ni−Ni bond.

Interactions between the d orbitals of two metal atoms brought close enough to each other to allow overlap would be expected to give rise to a manifold of bonding and antibonding orbital combinations, as shown in Scheme 1 in which D_{4h} symmetry is assumed.[3] Two d^8 Ni^{2+} ions provide 16 electrons with which to fill these eight molecular orbitals, resulting in the configuration $\sigma^2\pi^4\delta^2\delta^{*2}\pi^{*4}\sigma^{*2}$. With all of the bonding and antibonding levels filled, no net bonding results. Removal of one electron from the system changes this picture since the electron removed would be taken from an antibonding orbital. This would result in a species with a net bond order of $^1/_2$ and an unpaired electron in the σ^* orbital. However, the precise order of the MOs in Scheme 1 may vary depending on the metal[16] and the nature of the

Scheme 1

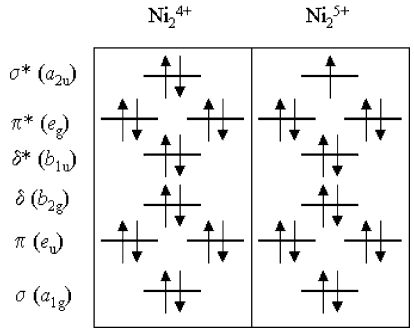

bridging ligands,[17] and the unpaired electron might occupy a different antibonding orbital. Among the factors lacking in the simple picture shown in Scheme 1 are the placement of ligand orbitals and possible mixing of the ligand π orbitals with the orbitals of the d manifold, which can cause ambiguity in the assignment of the electronic structure of the Ni_2^{5+} species.

For nickel, this question is particularly pertinent since it is known from X-ray spectroscopy that the d orbital manifold becomes significantly lower in energy toward the right side of the transition series.[18] When the d orbitals are lower in energy and thus closer to the energy levels of the filled ligand orbitals, it is more likely that mixing with ligand orbitals can occur.[19] It is even possible that the d orbitals might fall lower in energy than the filled ligand orbitals, and in such a situation, it might be difficult to discern whether oxidations are metal-centered or ligand-centered.

Our recent interest in the formation of nickel−nickel bonds from precursors that lack such bonds stems from our study of polynuclear complexes containing extended metal atom chains (EMACs),[20,21] where we discovered that linear Ni_3^{6+} complexes, which have been considered not to have Ni−Ni bonds,[22] can be oxidized to Ni_3^{7+} species with short Ni−Ni contacts very suggestive of Ni−Ni bond formation.[23] Extension of this concept to polynickel species having linear chains of five, seven, and nine Ni atoms has been achieved,[24] though one-electron-oxidation products of only the pentanickel

(11) (a) Millar, M.; Holm, R. H. *J. Am. Chem. Soc.* **1975**, *97*, 6052. (b) Herebian, D.; Bothe, E.; Neese, F.; Weyhermüller, T.; Wieghardt, K. *J. Am. Chem. Soc.* **2003**, *125*, 9116.
(12) In the latter case, DFT calculations show that the weak Ni···Ni interactions of 2.8 Å arise from a small but significant decrease of electron density from the Ni d_{z^2} orbitals (leading to partial Ni^{III} character for these ions, and therefore a partial bond). Wieghardt, K. personal communication.
(13) Oro, L. A.; Gómez-Beltrán, F.; Lahuerta-Peña, P.; González-Alvarez, D.; García-Fabián, L. *Rev. R. Acad. Cienc. Exactas, Fís., Quím. Nat. Zaragoza*, **1972**, *27*, 253.
(14) (a) Bellitto, C.; Dessy, G.; Fares, V. *Inorg. Chem.* **1985**, *24*, 2815. (b) Bellitto, C.; Dessy, G.; Fares, V. *Mol. Cryst. Liq. Cryst.* **1985**, *120*, 381.
(15) Cotton, F. A.; Matusz, M.; Poli, R.; Feng, X. J. *J. Am. Chem. Soc.* **1988**, *110*, 1144.
(16) Cotton, F. A.; Murillo, C. A.; Reibenspies, J. H.; Villagrán, D.; Wang, X. P.; Wilkinson, C. C. *Inorg. Chem.* **2004**, *43*, 8373.
(17) Cotton, F. A.; Gruhn, N. E.; Gu, J. D.; Huang, P.; Lichtenberger, D. L.; Murillo, C. A.; Van Dorn, L. O.; Wilkinson, C. C. *Science* **2002**, *298*, 1971.
(18) Shadle, S. E.; Hedman, B.; Hodgson, K. O.; Solomon, E. I. *J. Am. Chem. Soc.* **1995**, *117*, 2259.
(19) In fact, recent results from UV photoelectron spectroscopy suggest that the first ionization of dinickel formamidinates is ligand based and that the ligand orbitals are therefore situated higher in energy than the corresponding nickel orbitals. Lichtenberger, D. L. personal communication.
(20) Berry, J. F. In *Multiple Bonds between Metal Atoms*, 3rd ed.; Cotton, F. A., Murillo, C. A., Walton, R. A., Eds.; Springer Science and Business Media, Inc.: New York, 2005.
(21) Berry, J. F.; Cotton, F. A.; Daniels, L. M.; Murillo, C. A.; Wang, X. P. *Inorg. Chem.* **2003**, *42*, 2418.
(22) Clérac, R.; Cotton, F. A.; Dunbar, K. R.; Murillo, C. A.; Pascual, I.; Wang, X. P. *Inorg. Chem.* **1999**, *38*, 2655.
(23) Berry, J. F.; Cotton, F. A.; Daniels, L. M.; Murillo, C. A. *J. Am. Chem. Soc.* **2002**, *124*, 3212.
(24) (a) Shieh, S. J.; Chou, C. C.; Lee, G. H.; Wang, C. C.; Peng, S. M. *Angew. Chem., Int. Ed. Engl.* **1997**, *36*, 56. (b) Peng, S. M.; Wang, C. C.; Jang, Y. L.; Chen, Y. H.; Li, F. Y.; Mou, C. Y.; Leung, M. K. *J. Magn. Magn. Mater.* **2000**, *209*, 80. (c) Lai, S. Y.; Wang, C. C.; Chen, Y. H.; Lee, C. C.; Liu, Y. H.; Peng, S. M. *J. Chin. Chem. Soc.* **1999**, *46*, 477.

Scheme 2

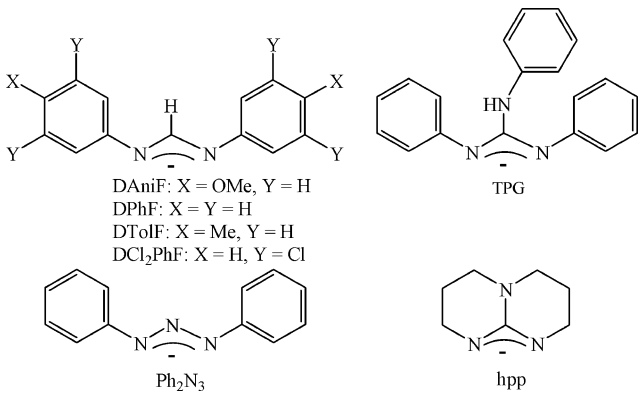

species have been studied in detail.[25] Recent DFT computational studies on these trinickel complexes have quite accurately reproduced the geometrical change in Ni···Ni separations between the neutral and one-electron-oxidized trinickel species but suggested that there is no net change in the Ni−Ni bond order of the two forms.[26] Instead, it was argued that both Ni_3^{6+} and Ni_3^{7+} complexes have a net bond order of $^1/_2$ and that the major change in Ni−Ni distances is due primarily to the concomitant removal of axial ligands upon one-electron oxidation.[26] A study of polynuclear Ni^{II} and Ni^{II}/Ni^{III} mixed-valence complexes during which there is no change in axial ligation is therefore quite desirable. We feel that understanding the simple dinuclear complexes is useful to provide some guidelines for the longer-chain species.

With these considerations in mind, we have begun an investigation of nickel complexes of type **III** with formamidinates and guanidinates in order to provide a more detailed picture of what happens upon oxidation of $Ni_2(ligand)_4$ complexes to $[Ni_2(ligand)_4]^+$ ions. The new complexes presented in this paper are $Ni_2(DAniF)_4$ (**1**), $[Ni_2(DAniF)_4]BF_4$ (**1-BF**$_4$), $Ni_2(TPG)_4$ (**2**), and $[Ni_2(TPG)_4]BF_4$ (**2-BF**$_4$). Comparisons will also be made with other known Ni_2 paddlewheel complexes with N-donor ligands: $Ni_2(DPhF)_4$[27] (**3**); $Ni_2(Ph_2N_3)_4$[28] (**4**); $Ni_2(DTolF)_4$[15] (**5**); $Ni_2(DCl_2PhF)_4$,[29] $Ni_2(MyBz)_4$,[30] and $Ni_2(hpp)_4$.[31] The ligands employed are shown in Scheme 2, and the abbreviation MyBz refers to *N*-myrtanylbenzamidinate.

Results and Discussion

Synthesis. The Ni_2^{4+} complex **1** was synthesized as previously reported,[29] while the guanidinato complex **2** was synthesized in good yields via a new route by reaction of $Ni(OAc)_2$ and molten HTPG at high temperature in a process that also liberates acetic acid, eq 1. Because **2** is stable to

$$2Ni(OAc)_2 + 4HTPG \rightarrow Ni_2(TPG)_4 + 4HOAc \quad (1)$$

air, it is straightforwardly purified by column chromatography.

Oxidation of **1** and **2** to their respective monocations (**1-BF**$_4$ and **2-BF**$_4$) is easily accomplished by the oxidant $AgBF_4$, according to eq 2. The silver metal byproduct was observed as a mirror which coated the bottom of the flask. For the oxidation of **2**, a brown precipitate was observed upon addition of $AgBF_4$ to an ether solution of **2**. However, it was not until this brown solid was dissolved in CH_2Cl_2 that silver metal precipitated from the reaction mixture. The brown intermediate is probably a silver complex in which the Ag^+ ions are coordinated by the free amine N atoms of the triphenylguanidinate ligand (eq 3). A similar silver intermediate has been reported in the process of oxidizing 1,1′-diacetylferrocene to the corresponding ferrocenium salt.[32]

$$Ni_2(DAniF)_4 + AgBF_4 \rightarrow [(Ni_2(DAniF)_4]BF_4 + Ag^0 \quad (2)$$

$$Ni_2(TPG)_4 + AgBF_4 \rightarrow \text{“}[AgNi_2(TPG)_4]BF_4\text{”} \rightarrow [Ni_2(TPG)_4]BF_4 + Ag^0 \quad (3)$$

It should be noted that solutions of **1-BF**$_4$ and **2-BF**$_4$ are not stable at room temperature and these compounds were crystallized at low temperatures. Oxidation of two additional dinickel complexes was also attempted during this work. The compounds $Ni_2(DPhF)_4$ (**3**) and $Ni_2(Ph_2N_3)_4$ (**4**) (DPhF = *N*,*N*′-diphenylformamidinate, and Ph_2N_3 = 1,3-diphenyltriazinate) both show reversible oxidation waves in their cyclic voltammograms at scan speeds of 100 mV s^{-1}, but the oxidized species which were generated either by Ag^+ or nitrosonium oxidation at −78 °C were too short-lived to be isolated. Nevertheless, since the crystal structures of **3** and **4** have been reported,[27,28] it is useful to include them in our discussion, as well as $Ni_2(DTolF)_4$ (**5**, DTolF = *N*,*N*′-di-*p*-tolylformamidinate), and the corresponding oxidized species (**5-BF**$_4$) which is also known.[15] The compounds $Ni_2(DCl_2PhF)_4$[29] and $Ni_2(hpp)_4$[31] have also been structurally characterized, though a reproducible synthetic procedure of the latter is not yet available.

Crystal Structures. The neutral Ni_2^{4+} complexes **1** and **2** crystallize as the halocarbon solvates **1**·1.5CH_2Cl_2 and **2**·4$CDCl_3$ (the latter having been crystallized after an NMR experiment), and both complexes show the typical lantern-type structure with the two nickel atoms being four coordinate (essentially square planar) and held together face-to-face by the four bridging ligands (see Figures 1 and 2). Geometrical parameters for the complexes are given in Table 1. Molecules of **1** reside on a crystallographic inversion center in the space group *Pccn*, and **2** contains a crystallographic 2-fold axis normal to the Ni···Ni vector in the space group *P*2/*n*. The Ni−N bond distances of 1.910[6] and 1.929[2] Å for **1** and **2**, respectively, are comparable to those in similar dinickel compounds,[15,27−29] and the two nonbonded

(25) Berry, J. F.; Cotton, F. A.; Lei, P.; Lu, T. B.; Murillo, C. A. *Inorg. Chem.* **2003**, *42*, 3534.
(26) Kiehl, P.; Rohmer, M. M.; Bénard, M. *Inorg. Chem.* **2004**, *43*, 3151.
(27) Arnold, D. I.; Cotton, F. A.; Maloney, D. J.; Matonic, J. H. *Polyhedron* **1997**, *16*, 133.
(28) Corbett, M.; Hoskins, B. F.; McLeod, N. J.; Oday, B. P. *Aust. J. Chem.* **1975**, *28*, 2377.
(29) Lin, C.; Protasiewicz, J. D.; Ren, T. *Inorg. Chem.* **1996**, *35*, 7455.
(30) Nelkenbaum, E.; Kapon, M.; Eisen, M. S. *J. Organomet. Chem.* **2005**, *690*, 3154.
(31) Cotton, F. A.; Murillo, C. A.; Timmons, D. J. unpublished results.
(32) Carty, P.; Dove, M. F. A. *J. Organomet. Chem.* **1971**, *28*, 125.

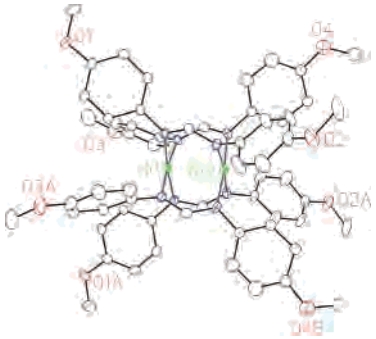

Figure 1. Molecule of **1** from **1**·1.3CH_2Cl_2 with displacement ellipsoids drawn at the 30% probability level and hydrogen atoms removed.

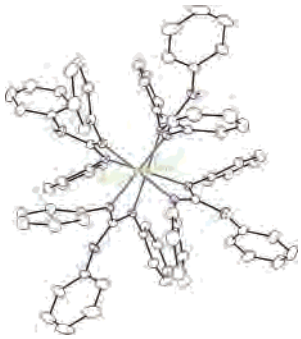

Figure 2. Molecule of **2** in **2**·4$CDCl_3$ with displacement ellipsoids drawn at the 30% probability level. Except for the amino hydrogen atoms, other hydrogen atoms have been removed.

Table 1. Selected Interatomic Distances and Angles (Å or deg) for **1**, **1-BF_4**, **2**, and **2-BF_4**[a]

compound	**1**·1.5CH_2Cl_2	**1-BF_4**·2CH_2Cl_2	**2**·4$CDCl_3$	**2-BF_4**·2CH_2Cl_2
Ni−Ni	2.476(1)	2.3703(4)	2.4280(5)	2.3298(6)
Ni−N	1.910[6]	1.909[2]	1.929[2]	1.921[2]
Ni−Ni−N	86.9[2]	88.46[6]	87.09[5]	88.90[5]
N−Ni−Ni−N torsion	15.6	14.1	19.9	15.7

Ni atoms are held together at distances of 2.476(1) Å in **1** and 2.4280(5) Å in **2**, and both are within the range of distances observed in other Ni_2^{4+} complexes.[15,27−29] The Ni atoms lie away from the center of the molecule and out of the square planes formed by the nitrogen atoms of the coordinated ligands by 0.103 and 0.098 Å in **1** and **2**, respectively, indicating a repulsive interaction between the nickel ions. This is in contrast to the dichromium tetraformamidinates[33] and tetraguanidinates,[34] in which a supershort Cr−Cr quadruple bond is formed. In these Cr_2^{4+} species, the two Cr atoms are also pulled out of the N_4 plane of the coordinated ligands but toward the centers of the molecules. This results in obtuse Cr−Cr−N angles of ∼95° in dichromium tetraguanidinates[34] and tetraformamidinates,[33] whereas the Ni···Ni−N angles are acute (86.9[2]° and 87.09[5]° in **1** and **2**, respectively.) Another important difference between the dinickel complexes **1** and **2** and their dichromium, dimolybdenum, or ditungsten analogues is that there is a significant twisting of the ligands resulting in large

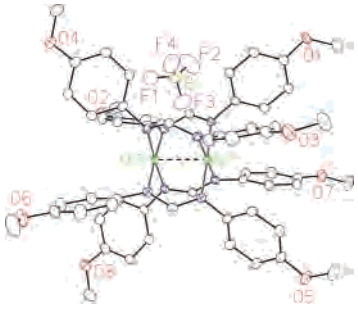

Figure 3. Thermal ellipsoid plot of **1-BF_4** from **1-BF_4**·2CH_2Cl_2 with ellipsoids drawn at the 30% probability level and hydrogen atoms removed.

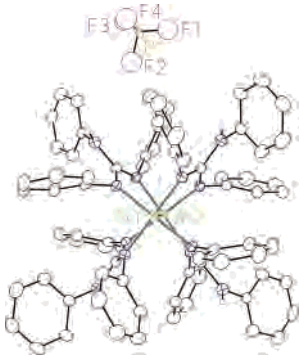

Figure 4. Thermal ellipsoid plot of **2-BF_4** from **2-BF_4**·1.25CH_2Cl_2 with ellipsoids drawn at the 30% probability level and only amino hydrogen atoms shown.

torsion angles (N−Ni···Ni−N) of 15.6° in **1** and 19.9° in **2**. Quadruply bonded Cr_2^{4+}, Mo_2^{4+}, and W_2^{4+} species do not have large torsion angles due to the stabilizing effect of the δ bond, which is highly sensitive to the torsion angle.[35]

The main features of the cationic species in the one-electron-oxidized complexes **1-BF_4**·2CH_2Cl_2 and **2-BF_4**·2CH_2Cl_2 (Figures 3 and 4) are similar to those in the neutral complexes in that the lantern-type dinickel core is retained. Similar to $[Ni_2(DTolF)_4]BF_4$,[15] the Ni−Ni distances in the oxidized complexes **1-BF_4** and **2-BF_4** of 2.3703(4) and 2.3298(6) Å, respectively, are significantly shorter than the Ni···Ni distances in the neutral species.[36] These changes are consistent with the removal of an electron from a Ni−Ni antibonding orbital, as will be described in more detail below. Interestingly, the shortening of the Ni−Ni distances upon oxidation (which we shall call Δd_{Ni-Ni}) for **1**/**1**$^+$ and **2**/**2**$^+$ (0.106(1) and 0.0982(6) Å, respectively) are significantly larger than Δd_{Ni-Ni} for **5**/**5**$^+$ (0.069(4) Å).[15] Other changes in the structures upon oxidation are to be noted: The Ni−N distances of 1.909[2] Å in **1-BF_4** are statistically the same as those of 1.910[6] Å found in **1**. In contrast, the Ni−N distances in **2-BF_4** of 1.921[2] Å are shorter than those of 1.929[2] Å in **2** by 0.008 Å, which is just above $3\sigma = 0.006$ Å and therefore significant. A decrease in M−N distances is expected if the dimetal core is oxidized since the charge of the dinuclear unit changes from 4+ to 5+, although these changes are often difficult to observe since the extra charge

(33) (a) Carlson-Day, K. M.; Eglin, J. L.; Lin, C.; Smith, L. T.; Staples, R. J.; Wipf, D. O. *Polyhedron* **1999**, *18*, 817. (b) Cotton, F. A.; Ren, T. *J. Am. Chem. Soc.* **1992**, *114*, 2237.
(34) Cotton, F. A.; Daniels, L. M.; Huang, P. L.; Murillo, C. A. *Inorg. Chem.* **2002**, *41*, 317.
(35) Cotton, F. A.; Nocera, D. G. *Acc. Chem. Res.* **2000**, *33*, 483.
(36) It should be noted that the Ni−Ni distances in these Ni_2^{5+} species are significantly shorter than those in $Ni_2(S_2CCH_3)_4I$ (2.514(3) Å). See ref 14.

Table 2. Structural and Electrochemical Information for Structurally Characterized Ni_2^{n+} ($n = 4$ and 5) Complexes

compound	$E_{1/2}$, V vs Fc/Fc^+	Ni_2^{4+} Ni···Ni, Å	Ni_2^{5+} Ni−Ni, Å	Δd_{Ni-Ni}, Å	ref
$Ni_2(Ph_2N_3)_4$	0.653	2.395(3)	–	–	28, this work
$Ni_2(DCl_2PhF)_4$	–[a]	2.462(1)	–	–	29
$Ni_2(DPhF)_4$	0.423	2.490(3)	–	–	27, 29
$Ni_2(DTolF)_4$	0.279	2.487[3]	2.418(4)	0.069(4)	15
$Ni_2(DAniF)_4$	0.207	2.476(1)	2.3703(4)	0.106(1)	29, this work
$Ni_2(MyBz)_4$	–	2.448(1)	–	–	30
$Ni_2(TPG)_4$	0.084	2.4280(5)	2.3298(6)	0.0982(6)	this work
$Ni_2(hpp)_4$	–	2.3764(9)	–	–	31

[a] Irreversible oxidation

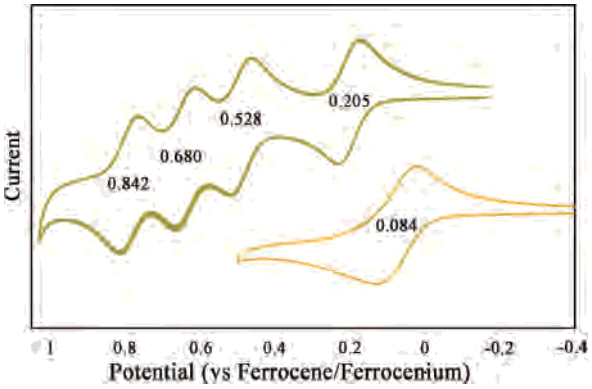

Figure 5. Cyclic voltammograms of **1** and **2** at a scan rate of 100 mV/s. $E_{1/2}$ values are given near the appropriate wave.

is spread over two metal atoms. As in their neutral counterparts, there are large torsion angles of 14.1° and 15.7° in **1-BF$_4$** and **2-BF$_4$**, respectively. Table 1 summarizes the bond distances and angles for **1**, **2**, **1-BF$_4$**, and **2-BF$_4$**.

Electrochemistry. There have been few reports of electrochemical data for lantern-type Ni_2^{4+} compounds with N-donor ligands. In the initial investigation of **5**,[15] a reversible one-electron oxidation wave was seen at 0.24 V (all potentials in this paper are reported vs ferrocene/ferrocenium). An irreversible wave at ca. 0.75 V was also noted. A more thorough electrochemical study of nine Ni_2(formamidinate)$_4$ compounds by Ren et al.[29] showed that the first oxidation potentials of these compounds are very sensitive to the nature of the ligands and that there is a strong correlation of the $E_{1/2}$ with the Hammett constant of the substituent in the diarylformamidinate ligands. The $E_{1/2}$ values changed from 0.207 V for the electron-donating *p*-anisyl derivative, compound **1**, to 0.867 V for the electron-withdrawing *m*-$CF_3C_6H_4$ derivative. For two compounds with ligands with even more electron-withdrawing capacity than the *m*-CF_3 derivative, namely, the *p*-CF_3 and the 3,5-Cl_2 derivatives, irreversible oxidation processes were observed. In no case was there a mention of any additional redox processes.

A reinvestigation of the redox behavior of **1** yielded a pleasant surprise. The cyclic voltammogram (shown in Figure 5) shows not one but *four* waves with profiles characteristic of reversible waves. The first wave at +0.205 V can be assigned to the $Ni_2^{4+/5+}$ process, and it is in essentially the same position as reported by Ren.[29] The additional waves at +0.528, +0.680, and +0.842 V must correspond to further oxidation processes not documented before.[37]

Compound **2** shows a more typical behavior in that its cyclic voltammogram consists of a single reversible oxidation wave at 0.084 V. However, this oxidation process is significantly more accessible than the corresponding $Ni_2^{4+/5+}$ couple in **1**. This is in agreement with the known ability of guanidinate ligands to stabilize dimetal complexes in higher than usual oxidation states.[38,39] However, whereas the dimolybdenum complex of triphenylguanidinate can be oxidized twice (first from Mo_2^{4+} to Mo_2^{5+} and then to Mo_2^{6+}),[39] there is no evidence for a second reversible oxidation in the dinickel complex **2**.[40]

The first oxidation potentials of all of the known structurally characterized Ni_2^{4+} complexes, along with selected structural information, are given in Table 2. Because no electrochemical data had been reported for the triazinato complex **4**, its cyclic voltammogram was measured, and it showed an oxidation process at 0.653 V. It is interesting to note that this potential is about 0.23 V higher than that of the formamidate analogue (0.423 V). Even though **4** exhibits one of the shortest nonbonded Ni···Ni distances known (2.395(3) Å), chemical oxidation did not provide any isolable product, possibly because of high reactivity of the oxidized product.

Electronic and EPR Spectroscopy. Spectroelectrochemistry is an excellent method for studying metal−metal-bonded complexes in various oxidation states,[41] thereby enabling a wealth of knowledge about the electronic structure of such species to be obtained because electronic spectra can be monitored during electrochemical oxidation or reduction. This technique was used to study the multiple redox processes (vide supra) in **1**. Only the first and second oxidation products (i.e., $\mathbf{1}^+$ and $\mathbf{1}^{2+}$) were stable enough in

(37) These waves correspond to a $Ni_2^{5+/6+}$ process and two ligand-based processes (see DFT section).

(38) Cotton, F. A.; Daniels, L. M.; Murillo, C. A.; Timmons, D. J.; Wilkinson, C. C. *J. Am. Chem. Soc.* **2002**, *124*, 9249.

(39) (a) Bailey, P. J.; Bone, S. F.; Mitchell, L. A.; Parsons, S.; Taylor, K. J.; Yellowlees, L. J. *Inorg. Chem.* **1997**, *36*, 5420. (b) Bailey, P. J.; Bone, S. F.; Mitchell, L. A.; Parsons, S.; Taylor, K. J.; Yellowlees, L. J. *Inorg. Chem.* **1997**, *36*, 867.

(40) The difference in the number of redox processes between **1** and **2** is attributable to difference in available electronic states for these compounds. For a discussion on the impact of the ligand on the available electronic states on the Ni_2 unit, see the DFT section.

(41) (a) Han, B. C.; Shao, J. G.; Ou, Z. P.; Phan, T. D.; Shen, J.; Bear, J. L.; Kadish, K. M. *Inorg. Chem.* **2004**, *43*, 7741. (b) Kadish, K. M.; Phan, T. D.; Wang, L. L.; Giribabu, L.; Thuriere, A.; Wellhoff, J.; Huang, S. R.; Van Caemelbecke, E.; Bear, J. L. *Inorg. Chem.* **2004**, *43*, 4825. (c) Kadish, K. M.; Phan, T. D.; Giribabu, L.; Shao, J. G.; Wang, L. L.; Thuriere, A.; Van Caemelbecke, E.; Bear, J. L. *Inorg. Chem.* **2004**, *43*, 1012. (d) Kadish, K. M.; Phan, T. D.; Giribabu, L.; Van Caemelbecke, E.; Bear, J. L. *Inorg. Chem.* **2003**, *42*, 8663.

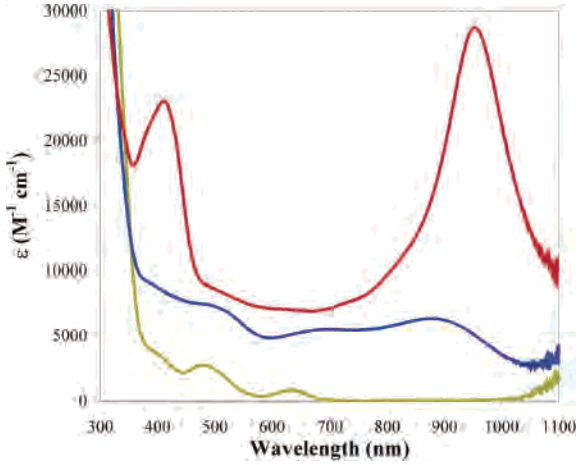

Figure 6. Electronic spectra of **1** (lower trace), **1-BF$_4$** (middle trace), and the Ni_2^{6+} species (upper trace) in CH_2Cl_2 solution at −25 °C. The latter two species were generated electrochemically.

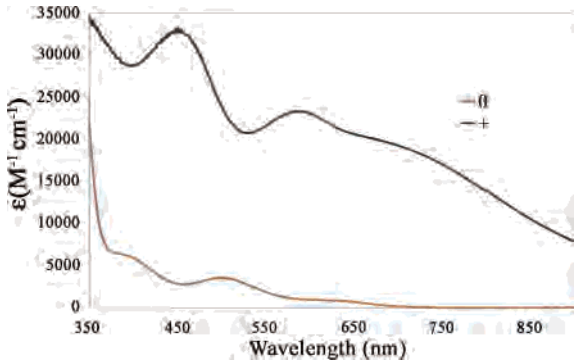

Figure 7. UV−visible spectra of **2** (upper trace) and **2-BF$_4$** (lower trace) in CH_2Cl_2 solution.

CH_2Cl_2 solution at −25 °C for their electronic spectra to be recorded (Figure 6). Attempts to generate the triply oxidized species showed non-isosbestic behavior in the monitored electronic spectra due to rapid decomposition of the species being generated.

The greenish-brown compound **1** shows three absorption maxima at 635, 485, and 400 nm in its electronic spectrum in the visible region. These all have molar absorptivities (ϵ) lower than 5000 M^{-1} cm^{-1}, though oxidation to $\mathbf{1}^+$ produces a black solution which shows maxima at 887, 690, and 500 nm, all of which have ϵ values larger than 5000 M^{-1} cm^{-1}, similar to the result reported for oxidation of **5**.[15] The most startling result, however, appears in the absorption spectrum of the doubly oxidized species, $\mathbf{1}^{2+}$, where a very intense band ($\epsilon \approx 30\,000$ M^{-1} cm^{-1}) in the near-IR is observed at 960 nm, as well as an intense transition at 415 nm ($\epsilon \approx 22\,000$ M^{-1} cm^{-1}). Thus, upon oxidation, there is an increase in intensity of the absorption spectrum, as well as a bathochromic shift of the lowest-energy bands. Because of the intensity of the bands in the electronic spectrum of $\mathbf{1}^{2+}$, it is reasonable to assign them to charge-transfer transitions.

The electronic spectra of **2** and **2-BF$_4$** were also measured in CH_2Cl_2 solution (Figure 7). While **2** is brown and exhibits maxima at 496 and 393 nm (both with $\epsilon \approx 5000$ M^{-1} cm^{-1}), **2-BF$_4$** is greenish-black and shows very intense bands at 711, 587, and 453 nm, all having ϵ values above 10 000 M^{-1} cm^{-1}, which identifies them as charge-transfer transitions. Interestingly, the electronic spectrum of **2-BF$_4$** is quite different from the spectrum of the corresponding formamidinato complex, **1-BF$_4$**. This difference is probably caused by the much higher basicity[42] of the guanidinate ligands relative to the formamidate ligands.

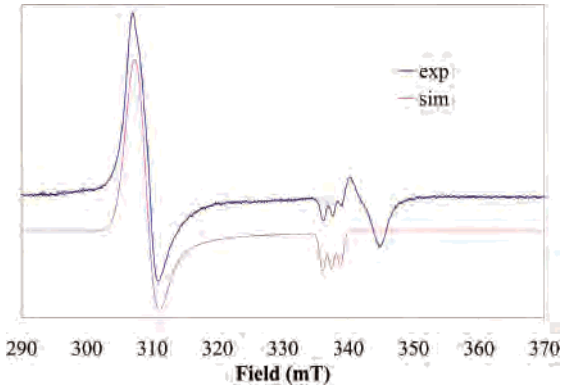

Figure 8. X-band EPR spectrum of **1-BF$_4$** in CH_2Cl_2 solution at 10 K. The upper trace corresponds to the experimental spectrum, while the lower trace is a simulation for the compound with an axial acetonitrile molecule (see text). The *A* value is 13 G. The signal with a *g* value of ca. 2.00 corresponds to an impurity.

The EPR spectrum of **1-BF$_4$** at 10 K, shown in Figure 8, has two components. The $g_\perp$ component appears at 2.234 and the $g_\parallel$ component at 2.045. The latter is partly overlapped by a somewhat broad, structureless signal at about $g = 2.0$ which may be due to contamination by an organic radical whose signal is broadened by interaction with a metal atom. The nature of this spectrum clearly establishes the presence of one unpaired electron on a Ni_2^{5+} core with, of course, partial delocalization into ligand orbitals. The triplet structure on the $g_\parallel$ signal was simulated using a molecule with an axially coordinated nitrogen atom of an acetonitrile molecule which is almost certainly carried over from the electrochemistry work that was performed in CH_3CN. The spectrum of **1-BF$_4$** is similar to that of **5-BF$_4$** where *g* values are $g_\perp = 2.210$ and $g_\parallel = 2.038$.[15] The isotropic *g* value obtained at room temperature for **2-BF$_4$**, 2.16, is just about that expected for the average of $g_\perp$ and $g_\parallel$ for **1-BF$_4$**: $(2 \times 2.23 + 2.04)/3 = 2.16$, which again supports the assertion that in these Ni_2^{5+} species the unpaired electron is mainly in metal-based orbitals.

Molecular Orbital Considerations. To better understand the quantitative calculations presented below, we must first make a qualitative survey of the molecular orbitals (MOs) involved. Those of the nickel atoms have already been presented in Scheme 1. It should be noted that the $d_{x^2-y^2}$ orbitals interact strongly with the σ orbitals of the ligands and they are not used in metal−metal bonding. Since ligand π orbitals may interact with the dimetal unit, they must also be considered in order to obtain an overall MO picture as they are bound to cause changes in the total MO diagram. The atoms of the N−C−N bridge form a π system which can be described in terms of N−C−N bonding, nonbonding, and antibonding interactions, as shown in Scheme 3.

(42) Bailey, P. J.; Pace, S. *Coord. Chem. Rev.* **2001**, *214*, 91.

Table 3. Calculated Geometries Using the Model $[Ni_2(HNCHNH)_4]^{0/+/2+}$

	Ni_2^{4+}		Ni_2^{5+}			Ni_2^{6+}	
	$^1A_{1g}$ 2-ζ	$^1A_{1g}$ 3-ζ	$^2A_{1u}$ 2-ζ	$^2A_{1u}$ 3-ζ	$^2A_{2u}$ 2-ζ	$^1A_{1g}$ (ligand oxidation)	$^1A_{1g}$ (nickel oxidation)
Ni−Ni, Å	2.569	2.547	2.565	2.547	2.445	2.554	2.327
Ni−N, Å	1.930	1.922	1.912	1.905	1.913	1.901	1.907
C−N, Å	1.321	1.314	1.324	1.377	1.318	1.328	1.315
C−H, Å	1.104	1.093	1.100	1.089	1.101	1.099	1.101
N−H, Å	1.016	1.008	1.020	1.011	1.017	1.025	1.021
relative energy (eV)	−	−	0	−	+0.30	0	+2.61

Scheme 3

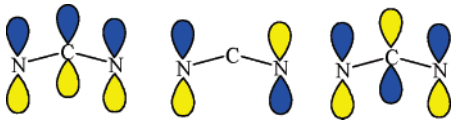

Scheme 4

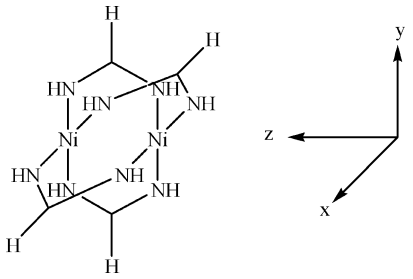

Since the $[N-C-N]^-$ formamidinate unit is a four-π-electron system, the antibonding combination on each ligand will be empty. These empty orbitals are presumably sufficiently high in energy that they can be disregarded. The filled bonding and nonbonding combinations, however, may fall within the energy range of the Ni_2 d manifold, and interactions between combinations of these orbitals and the Ni_2 d orbitals should be considered. To do this, a model $Ni_2(ligand)_4$ molecule of full D_{4h} symmetry in the coordinate system shown in Scheme 4 was used. In this coordinate system, the ligand π-bonding orbitals form combinations of a_{2g}, b_{2g}, and e_u symmetry and the nonbonding orbitals form combinations of a_{1u}, b_{1u}, and e_g symmetry.

The orbitals of the d manifold (Scheme 1) have the following symmetries in this coordinate system: σ, a_{1g}; π, e_u; δ, b_{2g}; δ^*, b_{1u}; π^*, e_g; and σ^*, a_{2u}. It can be envisioned that some of the metal-based orbitals may have significant interactions governed by symmetry with the π system of the coordinated formamidinate ligands. Such interactions may change the relative energies of the metal-based orbitals. When the symmetry is lowered from D_{4h} to D_4 (which results from nonzero torsion angles), the interactions will remain similar but the symmetry labels lose their gerade and ungerade subscripts.

Changes in the relative energies of the orbitals may also have important consequences for the electronic configuration of the oxidized species. Such variations in relative energy of the various orbitals may even generate oxidized species in which the oxidation is either metal-based or ligand-based. To differentiate between a ligand-based and a metal-based oxidation, DFT calculations were carried out. The theoretical results are compared to the experimental data below.

DFT Calculations. The first calculations were done on a simplified model of the neutral molecule, $Ni_2(HNCHNH)_4$. This model was used for both geometry and energy calculations at the B3LYP level using basis sets of double- and triple-ζ quality (see Experimental Section). In each case, the initial geometry was taken from the crystal structure coordinates, and the final geometry converged to a structure with D_{4h} symmetry. The calculated geometrical parameters are given in Table 3. The calculated Ni−N bond distances (1.930 Å from double-ζ, 1.922 Å from triple-ζ) reproduce very well the average value from the crystal structure of **1** (1.910[6] Å). However, the calculated Ni···Ni distances (2.569 Å from double-ζ and 2.547 Å from triple-ζ) are 0.07−0.09 Å longer than the experimental value (2.476(1) Å) in what appears to be a systematic overestimation.

The MO diagram in Figure 9 is based on the electronic structure calculated using the triple-ζ basis set and contains several features worth mentioning. To the left of the diagram, the orbitals of the d manifold (including the antibonding combination from the $d_{x^2-y^2}$ used in metal−ligand σ bonding) are listed, and the ligand π orbitals are shown to the right. Interactions between these sets of orbitals produce the MOs shown in the central section of the diagram. The σ and σ^* orbitals both appear to be substantially raised in energy through antibonding interactions (shown in Figure 9 with dotted red lines) with the σ orbitals of the bridging ligands (not shown in the picture). It is possible that these interactions may occur via overlap with the torus of the d_{z^2} orbitals. Strong π interactions (shown in green) also occur between

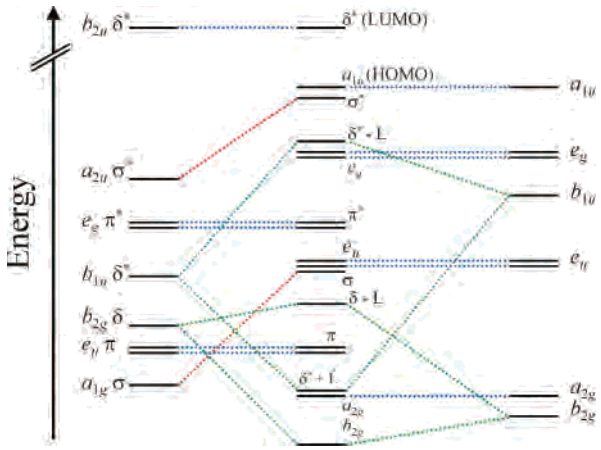

Figure 9. Molecular orbital diagram of $Ni_2(HNCHNH)_4$ species in D_{4h} symmetry showing interactions between the Ni_2 orbitals (far left) and the filled π orbitals of the ligand (far right). In the neutral dinickel complexes, all of the orbitals are filled except the top one (LUMO). Blue dotted lines indicate no interaction, red dotted lines indicate only a σ interaction, and green dotted lines indicate the π interactions.

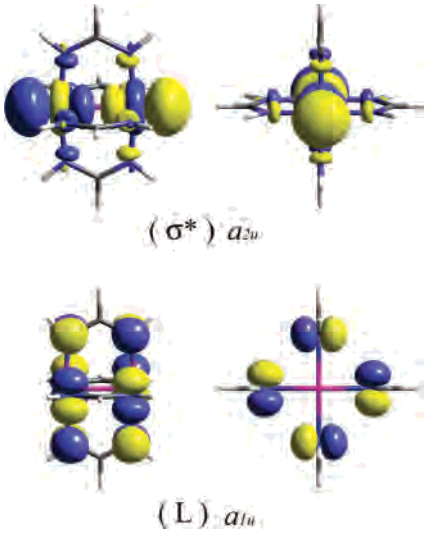

Figure 10. Depiction of the a_{1u} ligand orbital (bottom) and a_{2u} Ni_2 σ^* orbital (top) both viewed either from the side (left) or along the Ni−Ni vector (right).

the δ and δ^* orbitals of the Ni_2 manifold. The two highest occupied orbitals, a_{1u} and a_{2u}, are illustrated in Figure 10 to facilitate the discussion below.

The most striking result is that the HOMO is mainly ligand based. This would seem to imply that removal of one electron from the model species should give rise to a cation having one electron missing from the π orbitals of the ligand ($^2A_{1u}$). The geometry of this doublet state using the model cation $[Ni_2(HNCHNH)_4]^+$ has also been calculated from B3LYP using double-ζ and triple-ζ basis sets (Table 3). Importantly, the Ni···Ni and Ni−N distances are essentially the same as those calculated for the analogous neutral model (Table 3). Thus, it might seem that this simplified model does not reproduce the experimental data for **1**/**1**$^+$ where the Ni−Ni distance becomes shorter by 0.1 Å upon oxidation and where there is an EPR signal consistent with a metal-centered radical. However, the HOMO-1 of the neutral model is only 0.19 eV lower than the HOMO (for the 3-ζ calculation). This difference is within the uncertainties of the calculation. Moreover, even if the calculated order is correct, with such a small difference between the HOMO and HOMO-1, Koopmans' theorem is not to be trusted.[43]

The non-Koopmans $^2A_{2u}$ excited state, which represents the nickel-centered oxidation, was then calculated and its geometry was optimized.[44] The $^2A_{2u}$ state lies 0.3 eV (~2400 cm^{-1}) in energy above the ground doublet state, but the geometry of this state reproduces remarkably well the magnitude of the shortening of the Ni−Ni distances from **1** to **1**-BF_4 (0.105 Å). The calculated Ni−Ni distance of 2.445 Å is shorter than that calculated for the neutral complex by 0.13 Å.

It is therefore natural to ask why DFT did not straightforwardly predict the correct ground state for the $[Ni_2(HNCHNH)_4]^+$ model. An obvious part of the answer is that the ligand has been oversimplified and that by using the HNCHNH model ligand the $^2A_{2u}$ state has been disfavored.[45] To test this hypothesis, a computationally expensive single-point calculation employing the entire $Ni_2(DAniF)_4$ molecule as a model was made using the geometry observed in the crystal structure.[46] In Figure 11, the energies of the ligand-based a_{1u} orbital and the metal-based a_{2u} orbital for $Ni_2(HNCHNH)_4$ (double- and triple-ζ) and $Ni_2(DAniF)_4$ are compared. The ligand-based orbital (a_{1u}, shown in black) is greatly affected by changing of the basis set from double-ζ to triple-ζ, and the inclusion of the *p*-anisyl groups. The Ni_2 σ^* orbital, on the other hand, is only slightly raised in energy by changing the basis set from double-ζ to triple-ζ, and in the calculation of the full molecule, its energy is lowered again (since this calculation uses a double-ζ basis). The calculated HOMO/HOMO-1 energy difference becomes much smaller as a function of the basis set, as well as upon inclusion of the *p*-anisyl groups into the model. Furthermore, when the anisyl groups are included, the relative energies of these two orbitals are switched. The σ^* orbital becomes the HOMO, and the HOMO-1 is the a_{1u} ligand π orbital.[47] It should be mentioned that the very small energy difference (ΔE = 0.02 eV for the calculation of the full molecule) between the HOMO and HOMO-1 is consistent with the observation of four sequential reversible waves in the cyclic voltammogram of **1**. Because calculating the full $[Ni_2(DAniF)_4]^+$ cation as an open-shell system will be even more computationally expensive than for the neutral analogue, such a calculation was not attempted. However, results from the neutral compound suggest that if the full $[Ni_2(DAniF)_4]^+$ cation were to be calculated in a similar way, the resulting

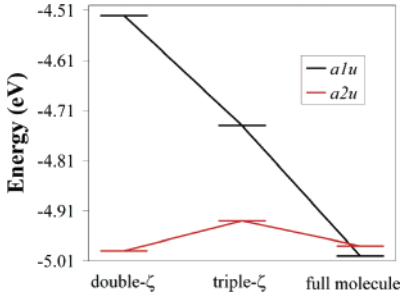

Figure 11. Variation of the energies of the highest two occupied MOs in $Ni_2(ligand)_4$ under different basis set conditions. Double-ζ and triple-ζ refer to the model complex $Ni_2(HNCHNH)_4$, whereas the results in the far right column are from a single-point calculation of the full $Ni_2(DAniF)_4$ molecule fixed at the geometry of the crystal structure. The symbol *a1u* refers to the ligand π orbital of a_{1u} symmetry, and *a2u* refers to the Ni_2 σ^* orbital.

(43) For an account on well-known violations of Koopmans' theorem, see for example: Ferreira, R. *Struct. Bond.* **1976**, *31*, 1.

(44) From this point onward, only the double-ζ basis set was used to allow swifter convergence and since the geometries calculated with the lager basis set are not significantly better in quality as compared to the experimental results.

(45) An indication that the nature of the substituents in the ligand has an important effect on the dimetal unit has been provided by the CVs of $Ni_2(formamidinate)_4$ compounds that showed a significant variation in the $E_{1/2}$ values as the value of the Hammet constant of the substituent is modified. See ref 29.

(46) Since the hydrogen atoms in the crystal structure are placed in calculated positions, the C−H bond distances are underestimated. Therefore, the hydrogen atom positions were optimized using the universal force field (UFF, see Experimental Section) keeping the rest of the structure fixed.

(47) It should be noted that a previous Xα calculation on a simplified model had shown that the odd electron in the oxidized complex was in an orbital of δ^* symmetry rather than one of σ^* symmetry. See ref 15

electronic state would correctly be assigned as the one in which one electron is removed from the Ni_2 σ^* orbital.

Additional support for the assignment of the $^2A_{2u}$ state as the ground state of the cation $[Ni_2(DAniF)_4]^+$ is provided by time-dependent DFT (TD-DFT). Calculations were performed to determine whether the features of the electronic spectrum of $\mathbf{1}^+$ could be modeled using either the $^2A_{2u}$ state or the $^2A_{1u}$ state. The lowest energy-allowed transition calculated for the $^2A_{1u}$ state is at 1205 nm (oscillator strength $f = 0.04$) and corresponds to excitations from the ligand π orbitals of e_g symmetry to the singly occupied a_{1u} ligand orbital, a process which can be essentially described as a ligand-to-ligand intervalence transition. For the $^2A_{2u}$ state, the lowest-energy band is calculated to be a Ni_2 $\pi^* \rightarrow \sigma^*$ transition at 874 nm ($f = 0.0002$). This value of 874 nm compares very well to the experimental value observed in **1-BF$_4$**, in which the lowest-energy band is at 887 nm with $\epsilon = 7500\ M^{-1}\ cm^{-1}$. The observed transition is too high in energy to be ascribed to an intervalence transition, as these bands typically appear in the NIR for ligand-based processes.[48] Thus, the band at 887 nm in **1-BF$_4$** should be attributed to a Laporte-allowed Ni_2 $\pi^* \rightarrow \sigma^*$ transition, and this assignment is consistent with a species that contains a Ni_2^{5+} unit and a bond order of $^1/_2$.

One of the advantages of DFT is that it can provide useful information about hypothetical compounds or those which are known to exist but cannot or have not been isolated. A good example is the doubly oxidized species generated from **1**, i.e., $[Ni_2(DAniF)_4]^{2+}$, which we have been unable to isolate in crystalline form, though its electronic spectrum in solution has been measured. Geometry optimization of the model complex $[Ni_2(HNCHNH)_4]^{2+}$ leads to a situation similar to that observed for $[Ni_2(HNCHNH)_4]^+$ and shows that the lowest-energy state is essentially the result of ligand oxidation (removal of two electrons from the a_{1u} orbital). Thus, the calculated geometrical values (Table 3) are similar to those for $Ni_2(HNCHNH)_4$ itself. In accord with all the preceding discussion, we suggest that here again the use of a simplified model does not reproduce experimental results and that there is actually a metal-based oxidation in **1-BF$_4$**. Support for this suggestion comes from a calculation of the geometry of the excited state of $[Ni_2(HNCHNH)_4]^{2+}$ which corresponds to the Ni_2^{6+} state having an empty σ^* orbital. The main difference in the geometry afforded by this calculation is that the Ni−Ni distance in such a Ni_2^{6+} state is 0.24 Å shorter than that in the neutral compound, a difference which is similar to that observed upon oxidation of $Pd_2(hpp)_4$ to $Pd_2(hpp)_4Cl_2$ (0.164 Å).[49] It should be noted, however, that the Ni_2^{6+} state is an excited state and is over 2 eV higher in energy than the ground state. For this reason, no TD-DFT calculations were attempted on it. For simplicity, we have not taken into account states in which one electron is removed from the metal and another is removed from the ligands due to the complexities involved in such states (they would necessarily be multideterminantal in nature). Therefore, at this time it is not possible to determine unambiguously the precise nature of the $[Ni_2(DAniF)_4]^{2+}$ cation. Nevertheless, by analogy to the singly oxidized compound, it may well contain a Ni_2^{6+} unit and it may have a Ni−Ni distance ~0.2 Å shorter than that in $Ni_2(DAniF)_4$. Thus, we could postulate a Ni−Ni single bond distance of ~2.25 Å.

Conclusions

New dinickel compounds with formamidinato and guanidinato ligands have been synthesized, and their one-electron-oxidation products, **1-BF$_4$** and **2-BF$_4$**, have been isolated and crystallographically characterized. Each complex shows a shortening of the Ni−Ni separation of about 0.1 Å upon oxidation, which is consistent with a metal-centered oxidation and formation of a Ni_2^{5+} species with a bond order of 1/2. Further evidence of this formulation is provided by EPR spectra of both species, for which isotropic g values of 2.171 and 2.160 are observed. The EPR spectrum of **1-BF$_4$** at 10 K shows distinct axial anisotropy, consistent with the presence of the unpaired electron in the Ni_2 σ^* orbital. A species with an Ni_2^{6+} core, observed by spectroelectrochemistry at −25 °C, is postulated to be the first lantern-type compound with a Ni−Ni bond order of one.

DFT calculations on the model complex $Ni_2(HNCHNH)_4$ reveal that the HOMO (a_{1u}, a ligand π orbital) and HOMO-1 (a_{2u}, the Ni_2 σ^* orbital) are close in energy, and the splitting between the two orbitals is basis set dependent. A single-point calculation of the full $Ni_2(DAniF)_4$ molecule results in an energy reversal of these two orbitals, suggesting that the HOMO of **1** is the Ni_2 σ^* orbital. This shows that results obtained using simplified models in DFT calculations should be treated with caution. Unfortunately, for large molecules, such models are the only practical approach.

Experimental Section

General. Unless specified otherwise, all manipulations were carried out under an atmosphere of dry nitrogen gas using standard Schlenk techniques. All solvents were either distilled over appropriate drying agents in a nitrogen atmosphere or purified by means of a Glass Contour solvent system. *N*,*N*′,*N*″-triphenylguanidine (HTPG) was purchased from TCI and used as received. Nickel acetate was synthesized by dissolving Ni powder in glacial acetic acid followed by crystallization. The dinuclear complex **1** was synthesized according to the method of Ren.[29]

Synthesis of [Ni$_2$(DAniF)$_4$]BF$_4$, 1-BF$_4$. To a mixture of $Ni_2(DAniF)_4$ (200 mg, 0.176 mmol) and $AgBF_4$ (38 mg, 0.19 mmol) was added 20 mL of dichloromethane. The resulting black mixture was stirred for 1.5 h and then filtered through Celite. The black solution was cooled to 0 °C and layered with cold hexanes. Crystals of $[Ni_2(DAniF)_4]BF_4 \cdot 2CH_2Cl_2$ grew within a week. Yield: 136 mg, 63%. IR (KBr, cm−1): 3301 w, 1688 m, 1604 m, 1500 s, 1460 w, 1343 w, 1293 m, 1252 s, 1183 w, 1083 m, 1026 s, 830 m, 585 w, 523 w. μ_{eff} (298 K) = 1.88 μ_B.

Synthesis of Ni$_2$(TPG)$_4$, 2. A flask was charged with $Ni(OAc)_2 \cdot 4H_2O$ (130 mg, 0.522 mmol) and 1.50 g (5.22 mmol) of HTPG. The solids were mixed at room temperature and then heated to 120 °C for 1 h while the flask was open to air. The mixture became brown. The residues were then cooled to room temperature, and

(48) See for example: Kokatam, S.; Weyhermüller, T.; Bothe, E.; Chaudhuri, P.; Wieghardt, K. *Inorg. Chem.* **2005**, *44*, 3709.
(49) Cotton, F. A.; Gu, J. D.; Murillo, C. A.; Timmons, D. J. *J. Am. Chem. Soc.* **1998**, *120*, 13280.

Table 4. Crystal Data for **1-BF$_4$**·2CH$_2$Cl$_2$, **2**·4CDCl$_3$, and **2-BF$_4$**·2CH$_2$Cl$_2$

	1-BF$_4$·2CH$_2$Cl$_2$	**2**·4CDCl$_3$	**2**-BF$_4$·2CH$_2$Cl$_2$
formula	$C_{62}H_{64}BCl_4F_4N_8Ni_2O_8$	$C_{80}H_{64}Cl_{12}D_4N_{12}Ni_2$	$C_{78}H_{68}BCl_4F_4N_{12}Ni_2$
fw	1395.24	1744.31	1519.47
cryst syst	triclinic	monoclinic	orthorhombic
space group	$P\bar{1}$	$P2/n$	$Aba2$
a (Å)	13.1601(8)	17.715(1)	17.592(1)
b (Å)	13.7494(9)	11.818(7)	18.815(2)
c (Å)	18.450(1)	18.648(1)	21.662(2)
α (deg)	99.574(1)	90	90
β (deg)	93.743(1)	90.039(1)	90
γ (deg)	92.096(1)	90	90
V (Å^3)	3281.2(4)	3904.2(4)	7170.0(1)
Z	2	2	4
d_{calcd} (g cm^{-3})	1.412	1.484	1.408
R1,[a] wR2[b]($I > 2\sigma I$)	0.0433, 0.1205	0.0390, 0.1047	0.0539, 0.1452
R1,[a] wR2[b](all data)	0.0506, 0.1255	0.0477, 0.1133	0.0705, 0.1589

[a] $R1 = \sum||F_o| - |F_c||/\sum|F_o|$. [b] $wR2 = [\sum[w(F_o^2 - F_c^2)^2]/\sum[w(F_o^2)^2]]^{1/2}$ and $w = 1/[\sigma^2(F_o^2) + (aP)^2 + bP]$, where $P = [\max(0 \text{ or } F_o^2) + 2(F_c^2)]/3$.

dichloromethane was used to extract the product. The extracts were concentrated and chromatographed on silica gel using dichloromethane as the eluent. The brown band, which was the first to clear the column, contained the product, and no other bands were collected. The crude product was then recrystallized several times in a mixture of CH_2Cl_2/hexanes, producing brown crystals. Yield: 118 mg, 50%. X-ray quality crystals were grown by slow evaporation of a $CDCl_3$ solution of **2** in an NMR tube (after an NMR spectrum had been taken). Anal. Calcd for $C_{76}H_{64}N_{12}Ni_2$: C 72.30, H 5.07, N 13.32%. Found: C 72.11, H 4.88, N 12.94%. ^{1}H NMR ($CDCl_3$, 300 MHz, δ): 4.862 (s), 5.921 (d, J = 8.1 Hz), 6.485 (m), 6.572 (m), 6.695 (br s), 6.856 (br s), 6.978 (m), 7.441 (br s), 7.924 (br s). ESI + mass spectrum (m/z, amu): 1262, M^+. IR (KBr, cm^{-1}): 3402 w, 3055 w, 1604 m, 1560 vs, 1525 w, 1475 s, 1421 s, 1374 m, 1302 w, 1264 m, 1210 w, 1176 w, 1073 w, 1027 w, 926 w, 837 w, 777 w, 749 m, 730 w, 693 m, 521 w, 485 w, 451 w. UV−vis, CH_2Cl_2 solution (λ_{max}, ϵ): 496, 5 × 10^3; 393, 8 × 10^3; 272, 2 × 10^5.

Synthesis of [Ni$_2$(TPG)$_4$]BF$_4$, 2-BF$_4$. To a solution of $Ni_2(TPG)_4$ (200 mg, 0.223 mmol) in 30 mL of Et_2O was added an Et_2O solution of $AgBF_4$ (43 mg, 0.22 mmol). A brown precipitate formed immediately. The mixture was filtered, and the brown solid was then treated with CH_2Cl_2 to give a black slurry. This was filtered through Celite to give a clear black solution, which was cooled to 0 °C, layered with cold hexanes, and kept in the freezer. Crystals grew within a week. Yield: 120 mg, 56%. IR (KBr, cm^{-1}): 3398 m, 3057 m, 1638 m, 1600 s, 1560 vs, 1482 vs, 1424 vs, 1375 m, 1304 m, 1265 m, 1208 w, 1175 w, 1061 m, 1056 m, 1023 m, 926 w, 833 w, 778 w, 752 s, 693 s, 515 w, 448 w. μ_{eff} (298 K) = 1.95 μ_B.

X-ray Crystallography. Suitable crystals of **1-BF$_4$**·2CH$_2$Cl$_2$, **2**·4CDCl$_3$, and **2-BF$_4$**·2CH$_2$Cl$_2$ were mounted and centered in the goniometer of a Bruker SMART 1000 CCD area detector diffractometer and cooled to −60 °C. Geometric and intensity data were collected using SMART software.[50] The data were processed using SAINT software,[51] and corrections for absorption were applied using the program SADABS.[52] A suitable crystal of **1**·1.5CH$_2$Cl$_2$ was mounted and centered on the goniometer of a Nonius FAST area detector system. Data were collected using the program MADNES[53] and processed using the program PROCOR.[54] An absorption correction was applied using the program SORTAV.[52] All structures were solved and refined using the SHELXTL program package.[55] Crystallographic data are listed in Table 4.

Physical Measurements. The IR spectra were taken on a Perkin-Elmer 16PC FTIR spectrometer using KBr pellets. Cyclic voltammograms were taken on a CH Instruments electrochemical analyzer using dichloromethane solutions with 1 M NBu_4PF_6 and 0.1 mM analyte. The electrodes were Pt disk (working), Pt wire (auxiliary), and Ag/AgCl (reference). The redox couple for ferrocene/ferrocenium consistently appeared at +450 mV under these conditions. Spectroelectrochemistry was performed at −25 °C using an EG&G potentiostat/galvanostat with 0.1 M NBu_4PF_6 with a Pt net working electrode, a Pt net auxiliary electrode, and an Ag/$AgNO_3$ reference electrode or alternatively in a thermostated optically transparent thin layer electrode (OTTLE) cell with CaF_2 windows. During coulometry, electronic spectra were monitored using an HP 8453 spectrophotometer (range: 190−1100 nm). Elemental analyses were carried out by Canadian Microanalytical Services in British Columbia, Canada. Samples were vacuum-dried prior to elemental analyses in order to remove the interstitial solvent molecules of the crystals. Samples of **1-BF4** and **2-BF4** sent for elemental analysis did not analyze well. We believe this is due to their thermal instability and that the samples decomposed during shipment. Magnetic susceptibility measurements were made on a Johnson Matthey magnetic susceptibility balance Mark II. ^{1}H NMR spectra were obtained on a VXR-300 NMR spectrometer. Mass spectrometry data (electrospray ionization) were recorded at the Laboratory for Biological Mass Spectrometry at Texas A&M University, using an MDS Series Qstar Pulsar with a spray voltage of 5 keV. Visible spectra were obtained on either a Shimadzu UV-2501 PC UV−vis spectrophotometer or a Cary 17D spectrophotometer.

Density Functional Calculations. DFT[56] calculations were performed with the hybrid Becke 3-parameter exchange functional[57] and the Lee−Yang−Parr nonlocal correlation functional[58] (B3LYP) implemented in the Gaussian 03 (Revision C.02) program suite.[59] For feasibility, the dinickel formamidinate molecules were represented by a model in which the aryl groups of the formamidinate

(50) *SMART*, 5.618; Bruker AXS, Inc.: Madison, WI, 1998.
(51) *SAINTPLUS*, 6.45A.; Bruker Analytical X-ray Systems, Inc.: Madison, WI, 1998.
(52) Blessing, R. H. *Acta Crystallogr., Sect. A* **1995**, *51*, 33.
(53) Messerschmitt, A.; Pflugrath, J. *J. Appl. Crystallogr.* **1987**, *20*, 306.
(54) (a) Kabsch, W. *J. Appl. Crystallogr.* **1988**, *21*, 67. (b) Kabsch, W. *J. Appl. Crystallogr.* **1988**, *21*, 916.
(55) Sheldrick, G. M. *SHELXTL97*; University of Göttingen: Göttingen, Germany, 1997.
(56) (a) Hohenberg, P.; Kohn, W. *Phys. Rev.* **1964**, *136*, B864. (b) Parr, R. G.; Yang, W. *Density-Functional Theory of Atoms and Molecules*; Oxford University Press: Oxford, 1989.
(57) (a) Becke, A. D. *Phys. Rev. A* **1988**, *38*, 3098. (b) Becke, A. D. *J. Chem. Phys.* **1993**, *98*, 1372. (c) Becke, A. D. *J. Chem. Phys.* **1993**, *98*, 5648.
(58) Lee, C. T.; Yang, W. T.; Parr, R. G. *Phys. Rev. B* **1998**, *37*.

ligands were replaced by hydrogen atoms, namely $Ni_2(HNCHNH)_4$. Double-ζ basis sets were used for the geometry-optimization calculations of the neutral, singly oxidized, doubly oxidized, and excited-state models of $Ni_2(HNCHNH)_4$, and triple-ζ basis sets were used in the neutral and singly oxidized models, as described in the discussion section. The double-ζ calculations consisted of the correlation-consistent polarized (cc-pVDZ)[60] valence basis set applied to the nonmetal atoms (carbon, nitrogen, and hydrogen), and an effective core potential (ECP) representing the 1s2s2p core was used for the nickel atoms along with the associated double-ζ basis set (LANL2DZ).[61] The triple-ζ calculations utilized the correlation consistent polarized (cc-pVTZ) basis set for nonmetal atoms and an EPC representing the 1s2s2p core along with the corresponding Stuttgart triple-ζ basis set[62] for nickel. For the all-atom single-point calculation of the $Ni_2(DAniF)_4$ molecule, the positions of all the non-hydrogen atoms were obtained from the crystal structure geometry. The hydrogen atoms were placed at positions calculated with the universal force field[63] (UFF) as implemented in the program Cerius.[64] Time-dependent[65] DFT calculations were performed by calculating the seven lowest excited states in all the neutral and singly oxidized calculations and the ground state of the doubly oxidized calculations to predict their electronic spectra. The self-consistent-field cycle convergence criterion on all calculations was increased from the default value to 10^{-8}. All calculations were run on an Origin 3800 64-processor SGI computer located at the Texas A&M Supercomputing facility.

Acknowledgment. We thank the National Science Foundation, the Robert A. Welch Foundation, and Texas A&M University for support. J.F.B. thanks the National Science Foundation for a predoctoral fellowship and the Alexander von Humboldt Foundation for a postdoctoral fellowship. We thank Petra Höfer and Frank Reikowski for assistance with the spectroelectrochemistry and EPR spectroscopy, respectively. We thank the Laboratory for Molecular Simulation at TAMU and especially Prof. M. B. Hall and Dr. L. M. Pérez for helpful discussions and software.

Supporting Information Available: Crystallographic data for **1**, **1-BF**$_4$, **2**, and **2-BF**$_4$ in cif format. This material is available free of charge via the Internet at http://pubs.acs.org.

IC060125Q

(59) Frisch, M. J.; Trucks, G. W.; Schlegel, H. B.; Scuseria, G. E.; Robb, M. A.; Cheeseman, J. R.; Montgomery, J. A., Jr.; Vreven, T.; Kudin, K. N.; Burant, J. C.; Millam, J. M.; Iyengar, S. S.; Tomasi, J.; Barone, V.; Mennucci, B.; Cossi, M.; Scalmani, G.; Rega, N.; Petersson, G. A.; Nakatsuji, H.; Hada, M.; Ehara, M.; Toyota, K.; Fukuda, R.; Hasegawa, J.; Ishida, M.; Nakajima, T.; Honda, Y.; Kitao, O.; Nakai, H.; Klene, M.; Li, X.; Knox, J. E.; Hratchian, H. P.; Cross, J. B.; Bakken, V.; Adamo, C.; Jaramillo, J.; Gomperts, R.; Stratmann, R. E.; Yazyev, O.; Austin, A. J.; Cammi, R.; Pomelli, C.; Ochterski, J. W.; Ayala, P. Y.; Morokuma, K.; Voth, G. A.; Salvador, P.; Dannenberg, J. J.; Zakrzewski, V. G.; Dapprich, S.; Daniels, A. D.; Strain, M. C.; Farkas, O.; Malick, D. K.; Rabuck, A. D.; Raghavachari, K.; Foresman, J. B.; Ortiz, J. V.; Cui, Q.; Baboul, A. G.; Clifford, S.; Cioslowski, J.; Stefanov, B. B.; Liu, G.; Liashenko, A.; Piskorz, P.; Komaromi, I.; Martin, R. L.; Fox, D. J.; Keith, T.; Al-Laham, M. A.; Peng, C. Y.; Nanayakkara, A.; Challacombe, M.; Gill, P. M. W.; Johnson, B.; Chen, W.; Wong, M. W.; Gonzalez, C.; Pople, J. A. *Gaussian 03*, revision C.02; Gaussian, Inc.: Wallingford, CT, 2004.
(60) Dunning, J., T. H. *J. Chem. Phys.* **1989**, *90*, 1007.
(61) (a) Wadt, W. R.; Hay, P. J. *J. Chem. Phys.* **1985**, *82*, 284. (b) Wadt, W. R.; Hay, P. J. *J. Chem. Phys.* **1985**, *82*, 299.
(62) Andrae, D.; Haussermann, U.; Dolg, M.; Stoll, H.; Preuss, H. *Theor. Chim. Acta* **1990**, *77*, 123.
(63) (a) Rappé, A. K.; Casewit, C. J.; Colwell, K. S.; Goddard, I., W. A.; Skiff, W. M. *J. Am. Chem. Soc.* **1992**, *114*, 10024. (b) Rappé, A. K.; Colwell, K. S. *Inorg. Chem.* **1993**, *32*, 3438.
(64) *Cerius2 Force-Field-Based Simulations*; Accelrys, Inc.: San Diego, 2001.
(65) (a) Stratmann, R. E.; Scuseria, G. E.; Frisch, M. J. *J. Chem. Phys.* **1998**, *109*, 8218. (b) Bauernschmitt, R.; Alrichs, R. *Chem. Phys. Lett.* **1996**, *256*, 454. (c) Casida, M. E.; Jamorski, C.; Casida, K. C.; Salahub, D. R. *J. Chem. Phys.* **1998**, *108*, 4439.